ACS OMEGA

http://pubs.acs.org/journal/acsodf

Article

Effect of Freeze–Thaw Cycles on Coal Pore Structure and Gas Emission Characteristics

Junwei Yuan, Jingyi Xia,* Yao Wang, Min Chen, and Jianxun Chen

Cite This: *ACS Omega* 2022, 7, 16087–16096

Read Online

ACCESS | Metrics & More | Article Recommendations

ABSTRACT: Here, we aim to clarify the influence of freeze–thaw cycle on pore structure and gas emission characteristics of coal body and to improve the application level of antipermeability and pumping technology based on freezing-induced cracking in a low-permeability coal seam. Freeze–thaw cycles of anthracite and coking coal were carried out in a freezer (−20 °C). Nuclear magnetic resonance was used to test the transformation characteristics of the freeze–thaw cycles on the pore structure of coal samples. The effect of freeze–thaw cycles on the gas emission characteristics of coal particles (1–3 mm) was studied using a self-built gas emission experimental platform (adsorption equilibrium gas pressure was 1.5 MPa). The results show that the pore structure of coal samples changes after the freeze–thaw cycle and the number of large pores and medium pores increases. The amount of gas emission, emission velocity, and gas diffusion coefficient of anthracite and coking coal all increase to different degrees after freeze–thaw cycles. The freeze–thaw damage of coking coal is greater than that of anthracite. In the third freeze–thaw cycle, the increase of each parameter is the largest, and the third freeze–thaw cycle is considered the optimal number of freezing–thawing cycles. The research results provide a theoretical basis for the production of low-permeability coal seam.

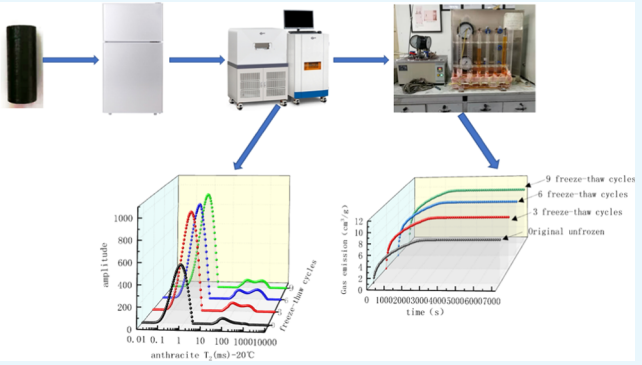

1. INTRODUCTION

China's coal resources are widely distributed and rich in reserves. However, with the deepening of mining depth, coal seam gas content and gas pressure continue to increase, and coal seam permeability gradually decreases, resulting in frequent coal and gas outbursts and other accidents. As a loose and porous medium, coal has a relatively developed pore-crack system, and gas is mainly adsorbed in the porous system of coal.[1] Therefore, reforming the pore structure of coal can effectively increase the permeability of coal seam, improve the effect of coal seam gas drainage, and effectively solve the problem of gas disasters. To effectively reduce the occurrence of gas disasters in coal mines, scholars at home and abroad have put forward technical measures such as protective layer mining,[2,3] hydraulic measures,[4−6] high-energy gas blasting,[7] static blasting,[8] and transformed the pore fissure system of coal so as to improve the permeability of coal seam and reduce the gas emission velocity and to effectively reduce the gas disasters in coal mines. However, there are some defects in the application of the above methods. It is urgent to study new methods of increasing permeability and promoting drainage in the coal seam, transforming the pore structure of coal, increasing the permeability of coal seam, and improving the effect of gas drainage, so as to effectively reduce the occurrence of mine gas disasters and accidents.

In terms of the influence of coal pore structure on gas emission characteristics, many scholars have carried out studies on the influence of coal samples with different metamorphic degrees on gas emission characteristics. Jiang[9,10] studied the relationship between coal pore structure parameters and gas emission characteristic parameters using Fourier tansform infrared spectroscopy and considered that low-grade coal has higher adsorption capacity and gas emission characteristics than medium-grade coal, which is prone to gas enrichment. Jia[11] studied pore characteristics of middle- and low-rank coal and its influence on gas emission characteristics in combination with fractal theory and believed that the initial gas emission velocity of middle- and low-rank coal was small, which decreased with the increase of fractal dimension and increased with the increase of average pore size.

In terms of pore structure transformation of coal by freeze–thaw cycle, many scholars at home and abroad have studied the

Received: March 9, 2022
Accepted: April 15, 2022
Published: April 27, 2022

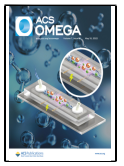

https://doi.org/10.1021/acsomega.2c01413
ACS Omega 2022, 7, 16087–16096

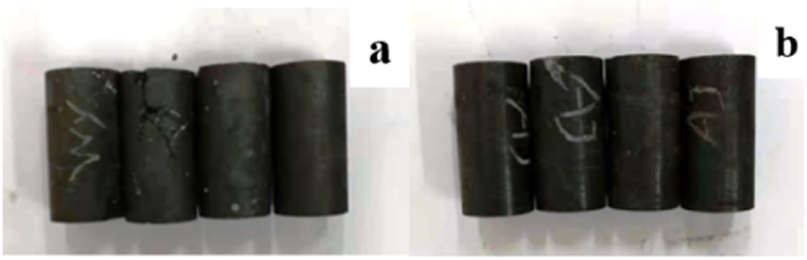

Figure 1. (a) Anthracite coal pillars and (b) coke coal pillars. (Photograph courtesy of Jingyi Xia. Copyright 2022. The figure is free domain).

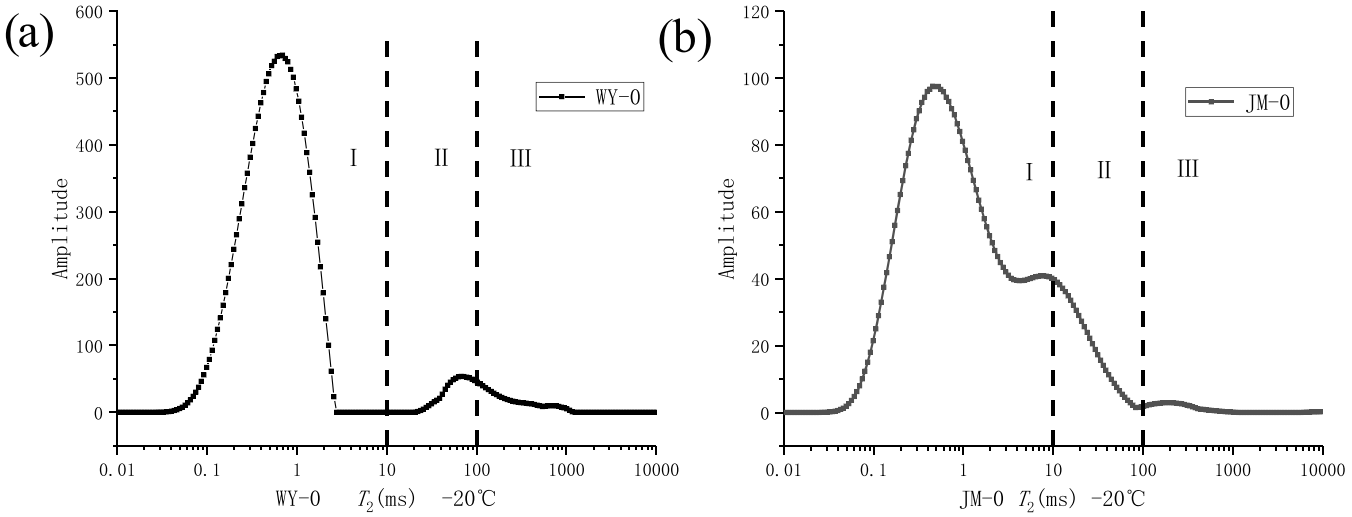

Figure 2. (a) Anthracite coal original T_2 spectrum and (b) coking coal original T_2 spectrum.

influence of freeze−thaw cycle on gas emission characteristics of coal, inspired by the damage phenomenon of rock and soil caused by freezing−thawing cycle in cold regions. Liu[12] and Everett[13] studied the influencing factors and mechanism of rock mass stability in the cold area under freeze−thaw cycle and showed that freeze−thaw temperature, saturation, and solution pH all cause damage to rock mass. Accordingly, many scholars applied freeze−thaw cycles to related studies of coal freezing cracking and achieved good research results. Xu[14] and Liu[15] analyzed the pore characteristics of coal samples after different freeze−thaw cycles using a sonic velocimeter and nuclear magnetic resonance equipment, indicating that freeze−thaw cycles can promote the development of various types of pores in coal samples and improve the connectivity of pores. Zhang[16−18] carried out the liquid nitrogen freezing test on anthracite and coking coal with ultrasonic waves. The results showed that the wave velocity of anthracite coal samples with water-saturated decreased, while the wave velocity of coking coal samples with water saturation increased. The liquid nitrogen freezing cracking effect of the water-saturated coal sample was better. Liu[19] studied the influence of liquid nitrogen cold leaching on the pore structure of different coal ranks. Uneven shrinkage occurred in coal, resulting in thermal stress greater than the tensile strength of coal. Zhai[20] analyzed the structural characteristics of coal pore distribution under the action of low-temperature freeze−thaw cycles. Yuan[21−23] analyzed the effect of liquid nitrogen freeze−thaw cycles on different coal ranks and tested the T_2 spectrum of water-saturated anthracite and coking coal samples under different freeze−thaw cycles. The results showed that freeze−thaw cycles promoted the development of internal pores in the coal samples and increased the number of internal pores in the coal samples. All of the above studies show that freeze−thaw cycles are beneficial to the pore structure of coal, but further research is needed on the pore structure transformation characteristics and gas emission characteristics of coal samples with different metamorphic degrees before and after freeze−thaw cycles. In this paper, the gas emission characteristics of coal samples before and after freeze−thaw cycles were studied through the self-built gas emission experimental platform, and the influence of freeze−thaw cycles on coal pore structure and gas emission characteristics was established, which laid a theoretical foundation for the application of new technology for increasing permeability and promoting drainage caused by freeze cracking.

2. COAL SAMPLE SELECTION AND RELATED PARAMETER DETERMINATION

2.1. Experimental Coal Sample. Anthracite and coking coal samples were selected as experimental coal samples. Among them, anthracite comes from the Guhanshan coal mine in Jiaozuo and coking coal comes from the main coking coal industry in Anyang city, Henan province. Z5040 vertical drilling machine was used to cut coal samples into cylindrical coal pillars with a diameter of 25 mm and a height of 50 mm in the laboratory. Anthracite coal sample numbers are WY-0, WY-3, WY-6, and WY-9, and coke coal sample numbers are JM-0, JM-3, JM-6, and JM-9, as shown in Figure 1.

2.2. Determination of Original NMR of Coal Samples. The measurement of original pore parameters of coal samples can provide a basis for exploring the pore transformation and gas emission characteristics of coal samples by freeze−thaw cycles. Compared with mercury intrusion, nitrogen adsorption, carbon

https://doi.org/10.1021/acsomega.2c01413
ACS Omega 2022, 7, 16087−16096

dioxide adsorption, small-angle scattering, micro-computed tomography (CT), optical microscopy, electron microscopes, etc., nuclear magnetic resonance (NMR) has the largest pore size applicable range. In the testing process, the NMR technology can penetrate deep into the coal without damaging the coal structure. The test is time-consuming, efficient, and convenient. Therefore, the NMR technology can more efficiently and accurately test the pore structure of the coal. Coal samples WY-0 and coal pillar JM-0 were tested by nuclear magnetic resonance, and the test results are shown in Figure 2.

2.2.1. T_2 Spectrum Analysis of Original Unfrozen Anthracite and Coking Coal. The T_2 spectrum of anthracite and coking coal shows a three-peak distribution. According to the research results of T_2 relaxation time and pore structure,[24] the T_2 relaxation time less than 10 ms represents micropores, the T_2 relaxation time between 10 and 100 ms represents medium pores, and the T_2 relaxation time greater than 100 ms represents large pores and fractures. Therefore, in this paper, the T_2 spectrum of coal samples is divided into three parts: I, II, and III, namely, $T_2 < 10$, $10 < T_2 < 100$, and $T_2 > 100$ ms. The higher the amplitude of T_2 spectrum, the larger the area of the corresponding map and the more the number of corresponding pore types in this area. It can be seen from Figure 2 that the total area of the T_2 spectrum of the anthracite coal sample is 17 217.9; the first peak area is 15 886.07, accounting for 96.265%; the second peak area is 1250.169, accounting for 7.261%; and the third peak area is 81.654, accounting for 0.474%. The first peak is all distributed in region I, a small part of the second peak is distributed in region II, and the rest and the third peak are distributed in region III. The first peak area of the T_2 spectrum of coking coal samples is the largest, and all of them are located in region I. The second and third peaks are mostly located in regions II and III, accounting for a large proportion of the total area, and the second peak accounts for 23.688%.

The proportion of the second and third peaks of coking coal is significantly greater than that of anthracite, indicating that the number of medium pores and large pores in coking coal is greater than that of anthracite. This is related to the metamorphic degree of coking coal and anthracite. The metamorphic degree of anthracite is higher than that of coking coal. The micropores in anthracite are more developed, while the medium pores, large pores, and fractures in coking coal are more developed.

3. EXPERIMENTAL EQUIPMENT AND PROCESS

3.1. Freeze−Thaw Cycle Experimental Device. The coal freeze−thaw cycles experiment system mainly includes four parts: dry weighing device, vacuum water-saturated device, freezer freeze−thaw device, and nuclear magnetic resonance testing device.

3.1.1. Dry-Weight Device. The dry-weight device consists of a drying oven and an electronic balance. The drying oven is a GRX-9053A hot air sterilization oven produced by Shanghai Yiheng Technology Co., Ltd., and the temperature of the drying oven is set to 105 °C. The electronic balance model is ME-T precision balance, its range is 0−220 g, and the precision is 0.1 mg.

3.1.2. Vacuum Water-Saturated Device. The vacuum water-saturated device mainly includes a vacuum pump and a water-saturated device. The vacuum pump model is a 2XZ-4 rotary vane vacuum pump, and the maximum vacuum pressure can reach −0.1 MPa.

3.1.3. Freezer Freeze−Thaw Device. The freezer freeze−thaw device consists of a freezer box and a thawing beaker. In this experiment, the coal samples are frozen in a freezer. The model of the freezer is BCD-58A118, the freezing temperature is −20°C, and the size of the freezer is $270 \times 350 \times 300$ mm^3. The beaker is a large-capacity vessel of volume 400 mL. After freezing, the coal samples are thawed naturally in a beaker at room temperature without airflow.

3.1.4. NMR Testing Device. The low-field nuclear magnetic resonance equipment adopts the MseoMR23-060H-I low-field nuclear magnetic resonance experimental system produced by Suzhou Niumai Technology Co., Ltd., including the host, display, test device, and test coil. The magnetic field strength of the equipment is (0.5 ± 0.05) T, the main frequency of the instrument is 21.3 MHz, and the system is equipped with two different sizes of coils, 25 and 50 mm. During the test, the saturated coal pillar sample needs to be placed in the coil and the 25 mm coil is used in this experiment.

3.2. Experimental Device for Gas Dispersion Characteristics. The gas emission characteristic experiment was carried out using a self-built gas emission experimental platform. The experimental platform mainly includes three parts: vacuum degassing system, quantitative charging system, and gas adsorption−desorption system. The equipment structure of the experimental platform for gas emission characteristics is shown in Figure 3.

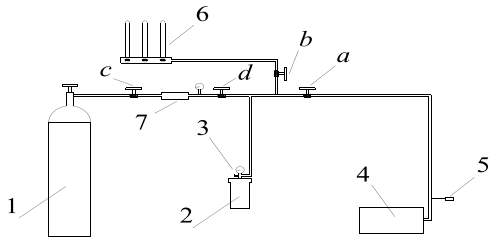

Figure 3. Structure diagram of gas emission experimental device. (1) High-purity gas steel tank, (2) adsorption coal sample tank, (3) pressure meter, (4) vacuum pump, (5) vacuum meter, (6) gas desorption apparatus, and (7) inflatable tank; (a−d) are valves.

3.2.1. Vacuum Degassing System. The system mainly evacuates and calibrates the space volume of coal sample tank, gas tank, and pipeline. It mainly includes a vacuum pump, composite vacuum gauge, coal sample tank, and experimental device pipeline. The vacuum degassing state of the coal sample tank can be determined by the composite vacuum gauge.

3.2.2. Quantitative Charging System. The system mainly evacuates the coal sample tank, the aeration tank, and the pipeline, and then fills the coal sample tank with methane gas. The amount of methane charged is controlled by the pressure gauge to ensure that the coal sample in the coal sample tank is balanced in the experimental requirements. The adsorption equilibrium was carried out under pressure. It mainly includes high-concentration gas steel tanks, precision pressure gauges, inflatable tanks, inflatable connecting pipes, and valves. The internal pressure of the methane steel tank is 16 MPa, the purity of CH_4 is 99.99%, the range of the precision pressure gauge is 4 MPa, and the minimum scale is 0.02 MPa.

3.2.3. Gas Adsorption−Desorption System. The system mainly measures the desorption process of the adsorption equilibrium coal sample. When the coal sample is in the adsorption equilibrium under the pressure required by the

https://doi.org/10.1021/acsomega.2c01413
ACS Omega 2022, 7, 16087−16096

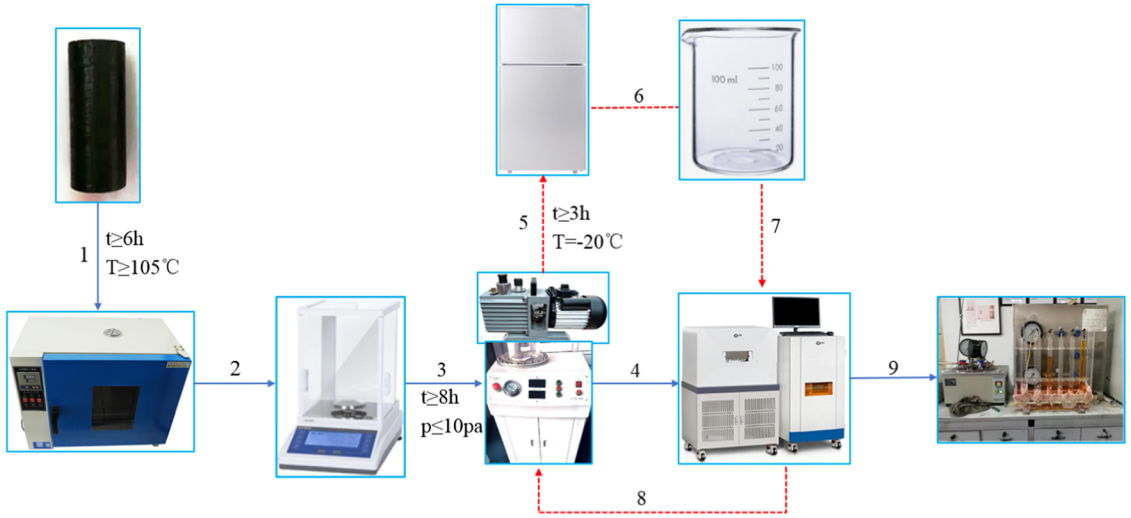

Figure 4. Experimental flowchart. (1) Coal sample drying, (2) measuring and weighing, (3) vacuum saturation, (4) original NMR test, (5) freezing, (6) thawing, (7) NMR test, (8) vacuum saturation, and (9) gas emission characteristics test. (Photograph courtesy of Jingyi Xia. Copyright 2022. The figure is free domain).

experiment, the desorption experiment is performed on the coal sample. It mainly includes coal sample tank, precision pressure gauge, and gas desorption instrument. The gas measuring device of the desorber consists of six glass measuring tubes, two of which have a measuring range of 800 mL and a minimum scale of 5 mL, and the other four glass measuring tubes with a measuring range of 300 mL and a minimum scale of 2 mL method to measure the volume of gas.

3.3. Experimental Process. The experimental flow of gas dispersion characteristics is shown in Figure 4, and the specific experimental flow is described as follows:

(1) The original coal samples numbered WY-0 and JM-0 were put into a drying oven, and the temperature was set at 105 °C. After every 6 h, they were taken out and weighed until the weight did not change and they were considered dry and taken out.

(2) The dried WY-0 and JM-0 were placed in the vacuum filling device for vacuum filling. The coal samples were put into the drying oven for vacuum filling, and the two groups of coal samples were vacuum-filled for more than 8 h under the pressure of 10 Pa to ensure that the coal samples were completely saturated. The coal pillar shall be put into the beaker with distilled water to ensure that all of the coal pillar is under the liquid level of distilled water. The beaker shall be put into the vacuum cover of the vacuum water saturation device and the switch of the vacuum water saturation device shall be opened for vacuumization.

(3) The water-saturated coal pillar was taken out, the surface moisture was dried, and WY-0 and JM-0 were tested by NMR. Nuclear magnetic resonance experiment operation steps: (a) Open the computer and NMR test system supporting software and set up the free induction decay (FID) sequence and the coil used; (b) turn on the radio frequency switch, connect the coil, put the coal sample into the coil, and set the relevant parameters of the instrument, as shown in Table 1; (c) carry out the operation steps of the experimental instrument calibration; and (d) after calibration, conduct a nuclear magnetic test on the coal sample.

Table 1. NMR Carr−Purcell−Meiboom−Gill (CPMG) Sequence Parameter List

parameter	numerical value	parameter	numerical value
SW (kHz)	333.333	DR	1
SF (MHz)	21	TW (ms)	1500
O_1 (Hz)	674 805	NS	64
RFD (ms)	0.08	PRG	1
RG1 (db)	15	P2 (μs)	11
P1 (μ)	6	TE (ms)	0.201
DRG	3	NECH	10 000

(4) After the nuclear magnetic resonance test, the coal samples were tested for gas emission characteristics. The coal samples were crushed with a ball mill and screened with a standard sieve of 1 and 3 mm to obtain particle coal samples with a particle size of 1−3 mm. The coal samples were put into a drying oven for drying, and the temperature was set at 105 °C. The samples were taken out and weighed every 6 h until the weight did not change. The treated coal sample was sealed in a drying dish for subsequent experiments.

(a) A group of 50 g coal samples were taken out of the drying dish and put into the clean coal sample tank. The coal samples were gently compacted and a layer of cotton was placed on the surface of the coal samples to prevent gas release during the experiment and bring coal particles into the experimental pipeline system, which blocked the experimental pipeline and affected the experimental results.

(b) A certain amount of methane was filled into the coal sample tank, the valve was closed, and the coal sample tank was put into water for 30 min. If there is no bubble in the coal sample tank, the air tightness is considered good. The water droplets on the surface of the coal sample tank were dried, and the coal sample in the coal sample tank was degassed by vacuum.

(c) The coal sample tank was filled with a gas of 99.99% purity, and the gas adsorption equilibrium pressure was set at 1.5 MPa. When the gas pressure of the

https://doi.org/10.1021/acsomega.2c01413
ACS Omega 2022, 7, 16087−16096

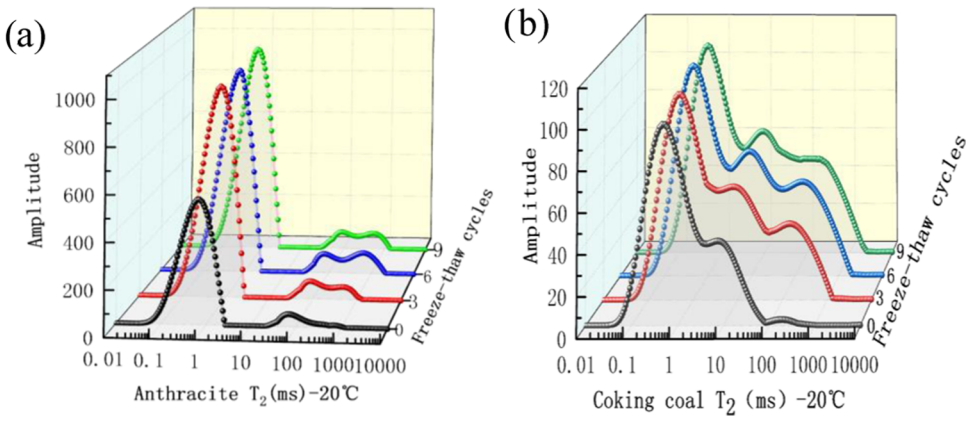

Figure 5. T_2 spectrum of (a) anthracite coal and (b) coking coal under different freeze−thaw cycles.

coal sample tank is slightly higher than the set balance pressure of 1.5 MPa, close the valve and stop filling the coal sample tank. After the coal sample was adsorbed for 12 h, methane gas was continued to be filled into the coal sample tank. When the gas pressure of the coal sample tank reaches the equilibrium pressure of 1.5 MPa set in the experiment and the number of pressure representations did not change in 3 h, the coal sample is considered to have reached the adsorption equilibrium.

(d) Open tossing in experiments of coal samples, coal sample tank valve, release the coal sample tank gas airbags to prepared in advance, when the pressure gauge reading fell to zero calibration, think the adsorption gas desorption, coal sample of coal and gas desorption test samples immediately device connection, record every minute parameters such as gas loss amount, the cumulative amount of gas radiation.

(5) WY-3 and JM-3, WY-6 and JM-6, and WY-9 and JM-9 are anthracite and coking coal samples of freeze−thaw times 3, 6, and 9, respectively. The six groups of coal samples underwent steps (1) and (2), drying and vacuum filling water. The moisture on the surface of the coal sample was wiped after vacuum water saturation and put into a sealed bag, and to ensure sealing, it was put into a freezer at −20 °C for 3 h. It was taken out, and then put in the beaker and thawed naturally at room temperature without airflow until the room temperature is completely restored. This is a freeze−thaw cycle. Three freeze−thaw cycles for WY-3 and JM-3, si freeze−thaw cycles for WY-6 and JM-6, and nine freeze−thaw cycles for WY-9 and JM-9;

(6) The WY-3 and JM-3, WY-6 and JM-6, and WY-9 and JM-9 after freeze−thaw cycles were subjected to nuclear magnetic resonance test and gas emission experiment according to steps (3) and (4).

4. ANALYSIS AND DISCUSSION OF FREEZE−THAW CYCLES ON GAS EMISSION CHARACTERISTICS OF COAL SAMPLES

The gas desorption volume measured in the experiment is converted to the gas desorption volume in the standard state, and the conversion equation is as follows

$$Q_t = \frac{273.2}{101325(273.2 + T)}(P_0 - 9.8h_w - P_s)Q_t' \quad (1)$$

where Q_t (mL/g) is the gas emission at time t in standard state, Q_t' (mL/g) is the gas emission amount at time t at the experimental ambient temperature T (in °C) is the experimental ambient temperature, P_0 (in Pa) is the atmospheric pressure of the experimental environment, h_w (in mm) is the height of the water column in the measuring cylinder when experimental data are read, and P_s (in Pa) is the saturated water vapor pressure at T temperature.

4.1. Analysis of Gas Emission from Coal Samples after Different Freeze−Thaw Cycles. After 0, 3, 6, and 9 freeze−thaw cycles of anthracite and coking coal, the pore structure of the coal samples was tested by NMR. The test results are shown in Figure 5.

4.1.1. Pore Changes of Coal Samples with Different Freeze−Thaw Times. After the anthracite and coking coal samples were frozen and thawed, the overall trend of the changes of each map in the T_2 spectrum of anthracite and coking coal was the same, showing an increasing trend.

(a) After the third freeze−thaw cycle, the change of the first peak of WY-3 coal sample increased, and the peak increased from 534 to 931, with an increase of 74.34%. The T_2 specturm area of anthracite increased from 17217.90 to 29829.08, with an increase of 73.24%.

(b) After the third freeze−thaw cycle, the T_2 spectrum area of JM-3 coal sample increased from 4886.01 to 9331.31, with an increase of 90.98%, which was significantly higher than that of anthracite coal sample. The first peak of the JM-3 coal sample changed slightly, but the total area of the second and third peaks increased from 1157.38 to 5513.05, an increase of 376.34%. The second peak and the third peak are located in areas II and III, which represent medium pores, large pores, and fractures, indicating that the number of medium pores, large pores, and fractures has increased significantly.

(c) After the sixth and ninth freeze−thaw cycles, the area and increase of T_2 spectrum of coal samples are shown in Table 2. It can be seen from Table 2 that the increase of the T_2 spectrum of WY-6, WY-9, JM-6, and JM-9 coal samples is significantly lower than that of WY-3 and JM-3, indicating that with the increase of freeze−thaw times, the transformation effect of freeze−thaw cycles on coal pore structure is gradually weakened, but on the whole, the number of micropores and medium pores of each coal

https://doi.org/10.1021/acsomega.2c01413
ACS Omega 2022, 7, 16087−16096

Table 2. Comparison of Peak and Area Changes of T_2 Spectrum of Coal Samples under Different Freeze−Thaw Cycles

coal	category	original values	9 freeze−thaw cycles	rate of change (%)
anthracite	first peak	15 886	22 508	41.68
	second peak	1250	4216	237.28
	third peak	82	3977	4750
	total map area	17 218	30 701	78.30
coking coal	first peak	3729	5751	54.22
	second peak	573	2379	315.18
	third peak	584	1973	237.84
	total map area	4886	10 103	106.77

sample is still increasing, and its growth rate is gradually decreasing.

The gas emission experiment was conducted on the tested coal samples, as shown in Figure 6. There were significant differences in the gas emission before and after freeze−thaw cycles of coal samples with different metamorphic degrees.

4.1.1.1. Comparison of Gas Emission of Unfrozen Coal Samples. With the increase in release time, the gas emission of unfrozen anthracite and coking coal increases rapidly first and then tends to be stable. Under experimental conditions, the maximum gas emission of anthracite is 7.53 cm^3/g and that of coking coal is 4.51 cm^3/g. The determination of pore parameters of the original T_2 spectrum of the coal sample in Figure 2 shows that the internal micropores and small pores of anthracite are more than those of coking coal. More micropores and small holes in coal make anthracite have strong adsorption capacity. Under the same adsorption conditions, anthracite can absorb more gas, resulting in its maximum release quantity in the desorption process being greater than coke coal.

4.1.1.2. Comparison of Gas Emission of Coal Samples with Different Freeze−Thaw Cycles. With the increase in the number of freezing−thawing cycles, the gas emission characteristic curves of the two coal samples move upward. Compared with the maximum gas emission of unfrozen, sixth, and ninth freeze−thaw cycles, the maximum gas emission of coal samples after the third freeze−thaw cycle increased the most. Compared with the original coal sample, the maximum gas emission of the anthracite coal sample increases by 23.24% and that of the coking coal sample increases by 25.06%. Under set experimental conditions, the maximum gas emission of different coal samples is shown in Table 3.

Due to the damage of coal matrix caused by freeze−thaw cycles, the pore structure of coal sample changes, and the number of micropores, small pores, and medium pores increases. Under the action of frost heaving force and thermal stress, the shrinkage and expansion of coal matrix lead to fatigue damage, and the internal moisture migration also causes shear damage to the pores of coal samples. More pores and fissures are generated in the coal matrix, and more gas is desorbed under the same desorption condition. The comparison of the gas emission of coal samples in the third, sixth, and ninth freeze−thaw cycles shows that the increase of the maximum gas emission of coking coal is always greater than that of anthracite. It shows that the damage of freeze−thaw cycles to coking coal is greater than that of anthracite, which causes more pores in coking coal, so the increase rate is large.

Table 3. Limit Gas Emission of Coal Pillar after Different Freeze−Thaw Times

coal sample number	maximum gas emission (cm^3/g)	amplification (%)
WY-0	7.53	
WY-3	9.28	23.24
WY-6	10.00	7.76
WY-9	10.25	2.5
JM-0	4.51	
JM-3	5.64	25.06
JM-6	6.12	8.51
JM-9	6.37	4.08

4.1.1.3. Analysis of the Relationship between Pore Parameters and Gas Emission in Coal Samples. After freeze−thaw cycles, the number of pores and the maximum amount of gas emission in the coal samples increase continuously. After the end of the ninth freeze−thaw cycle, the T_2 spectrum area of anthracite and coking coal increases by 78.30 and 106.77%, respectively, and the maximum gas emission increases by 36.12 and 41.24%, respectively. With the increase in the number of freeze−thaw cycles, the increase of the number of pores in the coal sample and the maximum gas emission decreases gradually, the upward movement of the gas emission decreases, and the maximum gas emission increases slowly. Therefore, there is a positive correlation between pore parameters of coal samples and gas emission, as shown in Figure 7.

4.2. Analysis of the Gas Emission Velocity of Coal Samples after Different Freeze−Thaw Cycles. Gas emission velocity is an important index parameter reflecting coal gas emission characteristics. For gas emission velocity, Yanas et al. believe that gas emission velocity changes with time in accordance with the law of power function

$$\frac{V_t}{V_a} = \left(\frac{t}{t_a}\right)^{-k_a} \tag{2}$$

where V_t ($cm^3/g{\cdot}min$) and V_a ($cm^3/g{\cdot}min$) are the gas emission velocities at time t and t_a, respectively, and k_a is the index affecting gas emission.

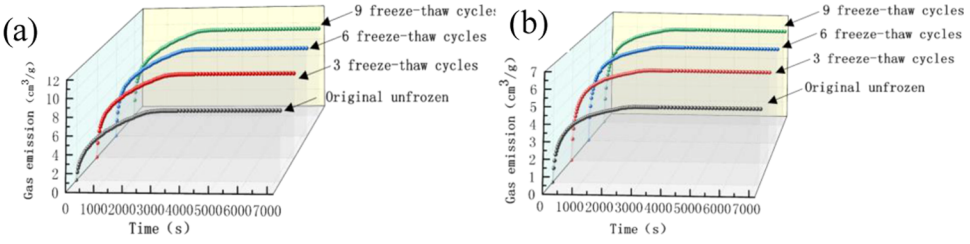

Figure 6. Variation curve of (a) anthracite coal and (b) coking coal gas emission under different freeze−thaw cycles.

https://doi.org/10.1021/acsomega.2c01413
ACS Omega 2022, 7, 16087−16096

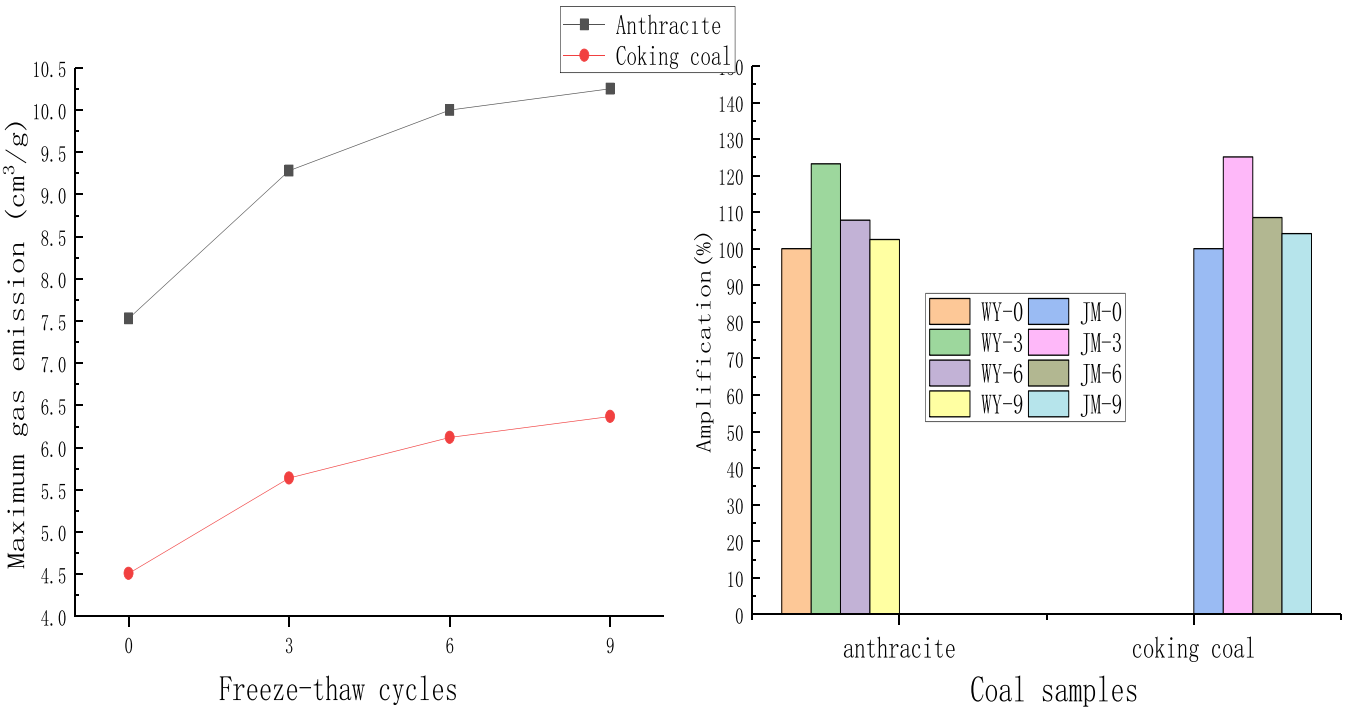

Figure 7. Maximum gas emission increment chart.

In this paper, the gas emission velocity was calculated according to the gas emission characteristic curve. Figure 8 is the gas emission velocity curve with time change of anthracite and coking coal samples with different freeze−thaw cycles.

As can be seen from Figure 8, the gas emission velocity of anthracite and coking coal before and after freezing−thawing gradually decreases with the extension of the emission time, forming a power exponential function change rule. At about 600 s before the coal sample starts to disperse, the velocity of the coal sample gas disperses sharply, but after 600 s, the velocity of the coal sample gas disperses slowly and gradually tends to be stable. In the first 600 s of the coal sample, the release velocity is fast, and its velocity attenuation changes dramatically, and it has the most obvious influence on gas outburst. Therefore, this paper focuses on analyzing the change rule of gas release velocity within 600 s.

4.2.1. Comparison of Gas Emission Velocity of Unfrozen Coal Samples. It can be seen from Figure 8 that the gas emission velocity of WY-0 and JM-0 coal samples decreases gradually with time and tends to be stable at 420 and 300 s, respectively. The time of gas emission velocity of anthracite tends to be stable is 120 s longer than that of coke coal. Anthracite coal and coking coal pore parameters, the anthracite within more pores, holes, has the stronger adsorption ability, in the same conditions can be more gas adsorption, therefore in the process of gas radiation have more sufficient gas basis and larger radiation resistance, make the anthracite coal sample gas radiation speed stabilizing time is longer than coking coal samples (see Section 2.2).

4.2.2. Comparison of Gas Emission Velocity of Coal Samples with Different Freeze−Thaw Cycles. It can be seen from Figure 8 that the gas emission velocity curves of each coal sample changing over time after freeze−thaw cycles are higher than that of the original coal sample, and the gas emission velocity curves of the coal sample move upward gradually with the increase in the number of freeze−thaw cycles. Freeze−thaw cycle also resulted in the changes of the internal pore structure of coal samples, coal can produce new and original cracks within interconnection, and coal permeability increase is good for the inside of the adsorption on coal gas desorption from coal and reduces the gas loss in the process of radiation resistance, so gas emission velocity of coal sample was greater than the original coal sample after freezing and thawing. The gas emission velocity of the first 120 s of the two coal samples was plotted, and Figure 9 is obtained as follows.

In the first 120 s, the gas emission velocity curves of the two unfrozen coal samples roughly overlapped, but with the increase in freezing−thawing time, the curves no longer overlapped, indicating that the gas emission velocity of anthracite was continuously greater than that of coke at any time.

4.3. Analysis of Gas Emission Coefficient of Coal Samples with Different Freeze−Thaw Cycles. Gas emission coefficient reflects gas emission velocity and emission capacity and is an important parameter to characterize gas emission obstruction in the coal matrix. In this paper, the linear diffusion theory and Fick diffusion law are used to calculate the gas diffusion coefficient. It is considered that the gas flow in granular coal obeys Fick's law, the diffusion flux is proportional to the concentration gradient, and the diffusion coefficient is a constant value, which is independent of the concentration, time, and coordinate. The movement of gas in coal cuttings with pore structure belongs to the spherical diffusion movement. According to the principle of continuity, the differential equation is established. The equation is as follows

$$\frac{\partial C}{\partial t} = D\left(\frac{\partial^2 C}{\partial r^2} + \frac{2}{r}\frac{\partial C}{\partial r}\right) \tag{3}$$

where D (m^2/s) is the diffusion coefficient, C (m^3/m^3) is the concentration of the diffused substance, R (in m) is the radius of coal particles, and T (in s) is the diffusion time.

After gas adsorption equilibrium of coal particles, its concentration is a certain value C_0. When coal particles are

https://doi.org/10.1021/acsomega.2c01413
ACS Omega 2022, 7, 16087−16096

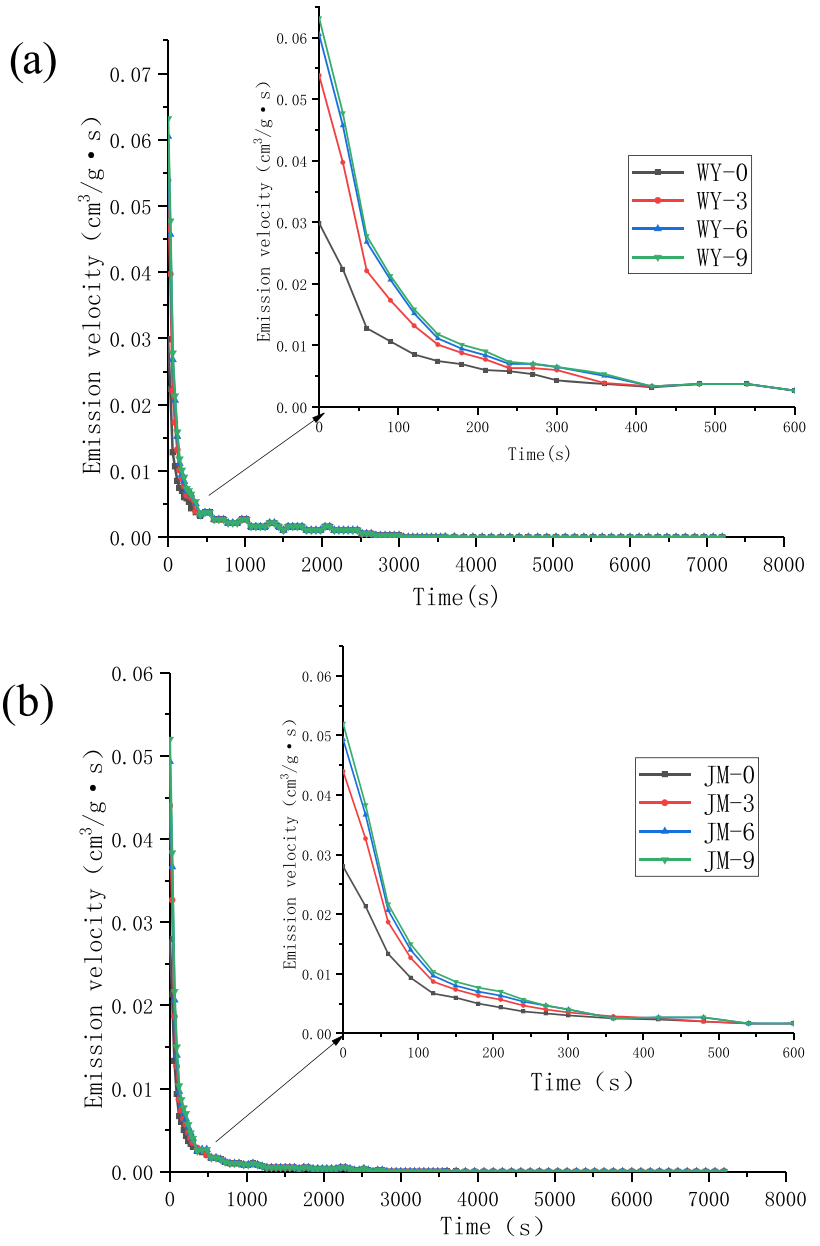

Figure 8. Gas emission rate of (a) anthracite coal and (b) coking coal with different freezing and thawing times.

exposed to atmospheric environment, the surface gas concentration decreases and the concentration gradient forms in the radius direction of the coal particles. The absorbed gas changes to a free state, and the gas diffuses from the center of coal particles to the surface with a constant surface concentration of C_1. The initial conditions and boundary conditions for the differential equation of gas spherical flow in coal particles are as follows

$$\begin{cases} c = c_0, & (0 \le r \le a, t = 0) \\ c = c_1, & (r = a, t > 0) \\ \dfrac{\partial c}{\partial r} = 0, & (r = 0, t > 0) \end{cases} \tag{4}$$

where c_0 (m^3/m^3) is the original gas concentration of coal particles, c_1 (m^3/m^3) is the gas concentration on the surface of coal particles, r is the radius of coal particles, and 2 mm is taken in this experiment.

Using Yang's method to solve the equation

$$\frac{Q_t}{Q_\infty} = \sqrt{1 - e^{-KD\pi^2/a^2}} \tag{5}$$

where Q_t (cm^3/g) is the cumulative gas emission amount at time t, Q_∞ (cm^3/g) is the maximum gas diffusion amount, K is the coefficient. The general value is 0.96.

The gas diffusion kinetic parameters of each coal sample have a high fitting correlation coefficient with Yang' s model. According to Young's model, the gas diffusion coefficient of coal samples with different freeze−thaw cycles is obtained as shown in Table 4.

The gas diffusion coefficient D of the coal samples increases to varying degrees after experiencing different freeze−thaw times, indicating that the freeze−thaw cycle is conducive to gas diffusion, which can effectively reduce the gas diffusion

https://doi.org/10.1021/acsomega.2c01413
ACS Omega 2022, 7, 16087−16096

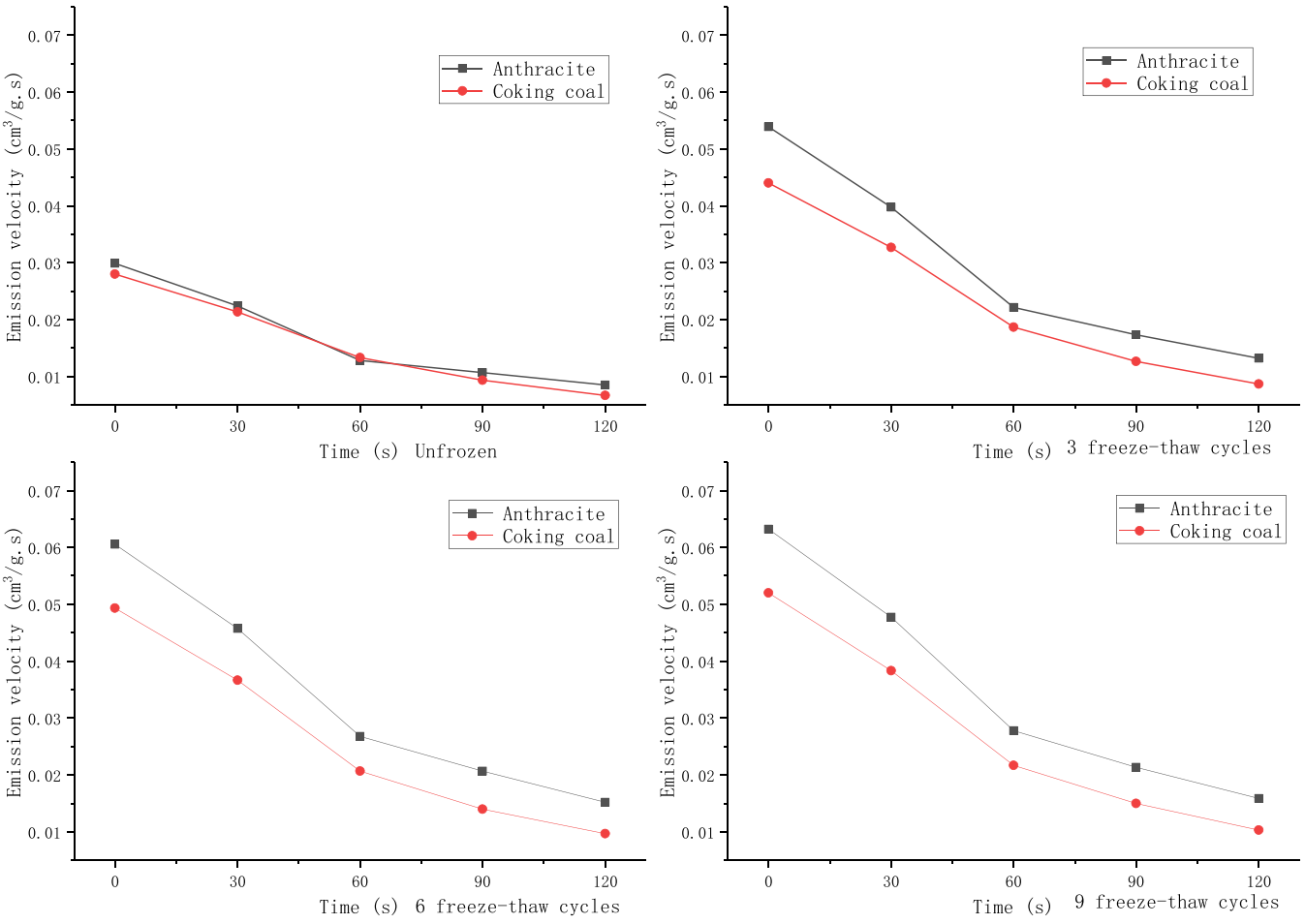

Figure 9. Gas emission velocity in 120 s under different freeze−thaw cycles.

Table 4. Fitting Data of Gas Diffusion Coefficient in Coal Pillars with Different Freezing and Thawing Times

step	fitting formula	gas diffusion coefficient D (cm^2/s)	ring-on-year growth (%)	R^2
WY-0	$\ln(1-(Q_t/Q_\infty)^2) = -1.40\times10^{-3}t + 0.50906$	5.916×10^{-6}		0.84748
WY-3	$\ln(1-(Q_t/Q_\infty)^2) = -1.51\times10^{-3}t + 0.4059$	6.381×10^{-6}	7.86	0.86271
WY-6	$\ln(1-(Q_t/Q_\infty)^2) = -1.525\times10^{-3}t + 0.36781$	6.444×10^{-6}	0.98	0.86771
WY-9	$\ln(1-(Q_t/Q_\infty)^2) = -1.53\times10^{-3}t + 0.29802$	6.465×10^{-6}	0.32	0.84581
JM-0	$\ln(1-(Q_t/Q_\infty)^2) = -2.09\times10^{-3}t + 0.21717$	8.832×10^{-6}		0.93955
JM-3	$\ln(1-(Q_t/Q_\infty)^2) = -2.37\times10^{-3}t + 0.21717$	10.015×10^{-6}	13.39	0.94746
JM-6	$\ln(1-(Q_t/Q_\infty)^2) = -2.41\times10^{-3}t + 0.21717$	10.184×10^{-6}	1.68	0.95052
JM-9	$\ln(1-(Q_t/Q_\infty)^2) = -2.42\times10^{-3}t + 0.21717$	10.226×10^{-6}	0.41	0.95142

resistance and make the gas more easily desorbed from the coal. It can be seen from Table 4 that in the third freeze−thaw cycle, the coal sample diffusion coefficient D increased the most; in the sixth and ninth freeze−thaw cycles, the gas diffusion coefficient still increased, but the increase was small. It shows that with the increase of freeze−thaw times, the influence of freeze−thaw cycles on gas diffusion coefficient of coal samples becomes less and less. The increase of gas diffusion coefficient of coke coal is larger than that of anthracite, which corresponds to the increase of gas emission, confirming that the damage of freeze−thaw cycles to coke coal is greater than that to anthracite.

5. CONCLUSIONS

(1) Under the present experimental conditions, the freeze−thaw cycle improves the gas emission amount, velocity, and gas diffusion coefficient of anthracite and coking coal and effectively improves the internal pore structure of anthracite and coking coal samples.

(2) With the increase in the number of freeze−thaw cycles (control the constant freezing−thawing time), the effect of freeze−thaw is obvious, and the increase is the largest in the third freeze−thaw cycle, while the increment decreases significantly in the sixth and ninth freeze−thaw cycles. Therefore, considering the coal mine site implementation and economic factors, three freeze−thaw cycles of coal samples can achieve the best effect, and the third freeze−thaw cycle is the best number of freeze−thaw cycles.

(3) After freeze−thaw cycle, the increase of gas diffusion coefficient of coke coal is obviously greater than that of anthracite, which proves that with the increase in freeze−thaw time, the increase of gas diffusion coefficient of coke

https://doi.org/10.1021/acsomega.2c01413
ACS Omega 2022, 7, 16087−16096

coal is greater than that of anthracite, indicating that the freeze−thaw damage of coke coal is greater than that of anthracite.

AUTHOR INFORMATION

Corresponding Author

Jingyi Xia − *School of Safety Science and Engineering, Henan Polytechnic University, Jiaozuo 454000, China;* orcid.org/0000-0001-5703-9828; Email: 279257963@qq.com

Authors

Junwei Yuan − *School of Safety Science and Engineering, Henan Polytechnic University, Jiaozuo 454000, China; MOE Engineering Research Center of Coal Mine Disaster Prevention and Emergency Rescue, Jiaozuo 454000, China; Collaborative Innovation Center of Coal Work Safety and Clean High Efficiency Utilization, Jiaozuo 454000, China*

Yao Wang − *School of Safety Science and Engineering, Henan Polytechnic University, Jiaozuo 454000, China;* orcid.org/0000-0001-7247-4019

Min Chen − *School of Safety Science and Engineering, Henan Polytechnic University, Jiaozuo 454000, China*

Jianxun Chen − *School of Safety Science and Engineering, Henan Polytechnic University, Jiaozuo 454000, China*

Complete contact information is available at: https://pubs.acs.org/10.1021/acsomega.2c01413

Notes

The authors declare no competing financial interest.

ACKNOWLEDGMENTS

This work was supported by the Key R&D and Promotion Projects in Henan Province (no. 202102310222).

REFERENCES

(1) Li, X. L.; Cao, Z.Y.; Xu, Y.L. Characteristics and trends of coal mine safety development. *Energy Sources, Part A* **2020**, 1−14.

(2) Liu, Q. J.; Fang, Y. Z.; Liu, F. Study on comparative analysis for protecting layer mining in closedistance coal seams and gas drainage effect. *Coal Technol.* **2022**, *41*, 159−162.

(3) Jiang, F. X.; Liu, Y.; Liu, J. Pressure-releasing mechanism of local protective layer in coal seam with rock burst. *Chin. J. Geotech. Eng.* **2019**, *41*, 368−375.

(4) Cao, Y. Research Status and Prospect of Coal and Gas Outburst Prevention and Control by Hydraulic Technology. *Saf. Coal Mines* **2020**, *51*, 60−66.

(5) Lu, Y.; Ge, Z.; Yang, F.; et al. Progress on the hydraulic measures for grid slotting and fracking to enhance coal seam permeability. *Int. J. Min. Sci. Technol.* **2017**, *27*, 867−871.

(6) Chen, X. J.; Du, Y. F.; Li, L. L. Study on comprehensive outburst elimination effect of hydraulic measures applied to coal mass. *Coal Sci. Technol.* **2017**, *45*, 43−49.

(7) Jia, T.; Huang, C. G.; Liu, G. J. Study on gas drainage boreholes with different space distances between boreholes affected to pre-cracking blasting enhancement effect of deep boreholes. *Coal Sci. Technol.* **2018**, *46*, 109−113.

(8) Liu, J.; Zhang, L.; Wei, Y.; Wu, Z. Coupling model of stress−damage−seepage and its application to static blasting technology in coal mine. *ACS Omega* **2021**, *6*, 34920−34930.

(9) Jiang, J. Y.; Cheng, Y. P.; Zhuang, S. Quantitative characterization of pore structure and gas adsorption and diffusion properties of low-rank coal. *J. China Coal Soc.* **2021**, *46*, 3221−3233.

(10) Qi, L.; Tang, X.; Wang, Z.; Peng, X. Pore characterization of different types of coal from coal and gas outburst disaster sites using low temperature nitrogen adsorption approach. *Int. J. Min. Sci. Technol.* **2017**, *27*, 371−377.

(11) Jia, X. M.; Lin, Y. B.; Ma, D. M. Pore Characteristics of Medium and Low Rank Coal and Its Influence on Gas Emission Characteristics. *Saf. Coal Mines* **2019**, *50*, 169−174.

(12) Liu, Q. S.; Huang, S. B.; Kang, Y. S.; Cui, X. Z. Advance and review on freezing-thawing damage of fractured rock. *Chin. J. Rock Mech. Eng.* **2015**, *34*, 452−471.

(13) Everett, D. H. The thermodynamics of frost damage to porous solids. *Trans. Faraday Soc.* **1961**, *57*, 1541.

(14) Xu, Y.; Huang, H.; Chu, Y. P. Research on evolution law of coal pore structure damage under the action of freeze-thaw. *Saf. Coal Mines* **2021**, *52*, 38−44.

(15) Li, X. L.; Chen, S. J.; Liu, S. M.; Li, Z. H. AE waveform characteristics of rock mass under uniaxial loading based on Hilbert-Huang transform. *J. Cent. South Univ.* **2021**, *28*, 1843−1856.

(16) Zhang, C. H.; Zhang, H. X.; Yu, Y. J.; et al. Effects of saturation and re-submersion on coal fracturing subjected to liquid nitrogen shock. *J. China Coal Soc.* **2016**, *41*, 400−406.

(17) Zhang, C. H.; Liu, P. S.; Wang, X. C. Contrast test study on fracturing anthracite and coking coal by liquid nitrogen cooling. *Coal Sci. Technol.* **2017**, *45*, 30−34.

(18) Zhang, C. H.; Guo, X. K.; Li, H. W. Study on influence of liquid nitrogen infiltration to saturated water coal fracture expanded. *Coal Sci. Technol.* **2016**, *44*, 99−105.

(19) Liu, S.; Li, X.; Wang, D.; Zhang, D. Investigations on the mechanism of the microstructural evolution of different coal ranks under liquid nitrogen cold soaking. *Energy Sources, Part A* **2020**, 1−17.

(20) Zhai, C.; Sun, Y. Experimental study on evolution of pore structure in coal after cyclic cryogenic fracturing. *Coal Sci. Technol.* **2017**, *45*, 24−29.

(21) Yuan, J. W.; Chang, D. Contrast test of liquid nitrogen freeze-thaw cycle cracking effect between anthracite and coking coal. *Coal Sci. Technol.* **2020**, *48*, 141−147.

(22) Yuan, J. W.; Xia, J. Y.; Chu, S. F. Transformation characteristics of pore structure of coal by freezing-thawing cycle. *Saf. Coal Mines* **2022**, *53*, 33−39.

(23) Yuan, J. W.; Yao, W.; Chen, X. J. Study on the Evolution of Pore Structure of Anthracite Coal under Liquid-Nitrogen Freeze-Thaw Cycles. *ACS Omega* **2022**, *7*, 4648−4654.

(24) Liu, J. J.; Hu, J. M.; Yang, M. Nuclear magnetic resonance experimental study on pore characteristics of high rank coal with different bedding. *China Saf. Sci. J.* **2021**, *31*, 83−89.